Journal of Air Pollution and Health (Spring 2025); 10(2): 243-268

Original Article

Available online at http://japh.tums.ac.ir

Investigating the rare phenomenon of dust in the southern shores of the Caspian Sea

***Zahra Ghassabi*[1], *Sara Karami*[2,*]**

[1] Atmospheric Hazard Forecast Group, Research Institute of Meteorology and Atmospheric Science (RIMAS), Tehran, Iran
[2] Air Pollution and Dust Research Group, Research Institute of Meteorology and Atmospheric Science (RIMAS), Tehran, Iran

ARTICLE INFORMATION

Article Chronology:
Received 29 December 2024
Revised 22 April 2025
Accepted 07 June 2025
Published 29 June 2025

Keywords:
Dust; Southern shores; Caspian sea; Hybrid single-particle lagrangian integrated trajectory (HYSPLIT); Cloud-Aerosol lidar and infrared pathfinder satellite observations (CALIPSO)

CORRESPONDING AUTHOR:
karamis.62 @gmail.com
Tel : (+98 21) 44787651
Fax : (+98 21) 44787670

ABSTRACT

Introduction: Climate change-driven droughts have intensified dust storms, expanding their impact to regions that previously experienced little to no dust. One such area is the southern shores of the Caspian Sea.

Materials and methods: This study investigated three severe dust cases along the southern Caspian coast, originating from various sources both inside and outside of Iran. A combination of satellite data, reanalysis data, and numerical model outputs was analyzed. The dust surface concentration output from the WRF-Chem model's 36- and 48-h forecasts was qualitatively compared with the dust patterns from MERRA2 reanalysis data.

Results: Cloud-Aerosol Lidar and Infrared Pathfinder Satellite Observations (CALIPSO) satellite data confirmed the presence of dust from near the surface to over 5 km in altitude, allowing dust to cross the Alborz range. Satellite imagery and Hybrid Single-Particle Lagrangian Integrated Trajectory (HYSPLIT) model outputs revealed that dust over the southern Caspian coast originated from three sources: northern Iraq, central Iran, and western Turkmenistan. Comparing Weather Research and Forecasting (WRF)-Chem model outputs with reanalysis data demonstrated that the model accurately predicted dust events along the southern Caspian shores in all three cases, though its precision is not yet suitable for quantitative comparison.

Conclusion: According to the results of this study, dust in the northern provinces of Iran is emitted from three dust sources in northern Iraq, central Iran, and Turkmenistan. Also, the WRF-Chem model has been able to predict the dust transport from these different dust sources to northern Iran. However, it can be stated that the accuracy of the outputs is still not suitable for quantitative comparison.

Please cite this article as: Ghassabi Z, Karami S. Investigating the rare phenomenon of dust in the southern shores of the Caspian Sea. Journal of Air Pollution and Health. 2025;10(2): 243-268.
https://doi.org/10.18502/japh.v10i2.19079

Introduction

An increase in surface dust concentration has adverse effects on the living organisms health, socio-economic sectors, and transportation systems [1-3]. Recent changes in the frequency of dust storms have amplified these consequences, particularly in terms of public health [4]. Economically, dust storms negatively impact solar electricity production, agriculture, industrial productivity, and cause damage to agricultural land, buildings, and infrastructure [5-7].

In Iran, the southwestern and western regions are most frequently affected by dust storms due to their proximity to major dust sources and their location in key entryways for dust [8, 9]. However, central and northern parts of the country also experience dust events, albeit less frequently [10, 11]. Despite the northern regions of Iran, particularly the southern shores of the Caspian Sea being characterized by a mild, humid climate and significant rainfall due to the Alborz mountain range, dust events in these areas are typically rare. Nevertheless, recent data show an increasing trend in dust activity in this region [12-14].

Some of the dust particles over the southern shores of the Caspian Sea originate from Turkmenistan. The formation of a thermal cyclone over a warm temperature core in the eastern Caspian Sea, along with the resulting surface convergence, transports dust into the atmospheric column. The relative atmospheric stability in the middle and upper levels prevents the dust from dispersing vertically in the troposphere, confining it to altitudes below 700 hPa. An increase in 10 m wind speed, driven by a growing pressure gradient over the desert areas east of the Caspian Sea, generates northeasterly currents that carry dust toward the southern coasts of the Caspian Sea [15].

Dust from Iran's western neighboring countries can also affect the Caspian Sea. Although, the investigation of the Aerosol Optical Depth anomaly (AOD) compared to the long period has shown that the dust particles transfer from east of Iraq and reaching the Caspian Sea is not a common phenomenon [16]. In a case study the dust transport from Iraq to the north west of Iran was so severe, so that many provinces in this area were affected by the dust [17, 18] identified three main pathways for dust entering western Iran: (1) a northwest-southeast path from northwestern Iraq and southeastern Syria into western Iran, (2) an east-west path from the Iraq-Jordan border to western Iran, and (3) a south-north flow from the southern shores of the Persian Gulf to western Iran.

Synoptic patterns play a crucial role in transporting dust to the southern coast of the Caspian Sea. A study on dust risk in the southwestern areas of the Caspian Sea identified two key patterns contributing to dust events in the region. The first pattern occurs in spring, when Sudanese low-pressure systems and active low-pressure systems over Iraq and northeastern Africa drive dust into the area. The second pattern takes place in summer, when thermal low-pressure systems over Pakistan are responsible for dust transport into the region [19].

The dust phenomenon, once unfamiliar to the residents of northern Iran, has recently led to significant reductions in horizontal visibility in these areas. The purpose of this study is to investigate the occurrence of dust events in northern Iran, identify active dust sources, and explore the factors contributing to the transport of dust particles to this region.

Materials and methods

In this study, three cases of severe and widespread dust events along the southern shores of the Caspian Sea, which occurred in 2022, were investigated. First, to examine the dust patterns in the region, true-color images from MODIS/ Terra were analyzed. Then, data on present

weather codes, horizontal visibility, and 10-m wind direction and speed from meteorological stations in northern Iran, which reported dust-related weather codes (6 and 7), were examined. Dust RGB images from the MSG satellite were analyzed at different hours of the day to investigate the dust transport over the region. To explore the vertical distribution of dust particles in the atmosphere, various Cloud-Aerosol Lidar and Infrared Pathfinder Satellite Observations (CALIPSO) satellite products were used. Aerosol Optical Depth (AOD) data from MODIS/Terra were also analyzed to assess the concentration of dust and aerosols in the atmosphere during each case study.

Synoptic analysis was performed using data on Mean Sea Level Pressure (MSLP), 10 m wind velocity, temperature, geopotential height, and relative humidity at 850 hPa, as well as geopotential height at 500 hPa. Maps were generated using ECMWF data with a horizontal resolution of 0.75 degrees.

To detect particle trajectories, the Hybrid Single-Particle Lagrangian Integrated Trajectory (HYSPLIT) trajectory model was run in backward mode for a location on the southeastern Caspian coast at an altitude of 100 m. For meteorological data, GFS reanalysis data with a horizontal resolution of 0.25 degrees were used. The height of 100 m was chosen because much of the study area is situated on the Caspian Sea and its coastal regions, which have low elevation above sea level. To further investigate particle paths and their spatial and temporal distribution in the atmosphere, the HYSPLIT dispersion model was also applied using the same meteorological data.

To evaluate the feasibility of forecasting dust along the southern Caspian coast, the Weather Research and Forecasting (WRF)-Chem model was run using GFS forecast data with a horizontal resolution of 0.25 degrees for initial and boundary conditions on a grid with 21 km resolution. Some schemes used in the WRF-Chem model implementation are shown in Table 1.

Table 1. Some schemes used in the WRF-Chem model

Microphysics	WRF Single-Moment 5-class scheme [20]
long wave radiation	RRTM scheme [21]
short wave radiation	Goddard shortwave [22]
Surface physics	Noah Land Surface Model [23]
Boundary layer	Yonsei University scheme [24, 25]
Cumulus diagram	Grell 3D [26]
dust emission	AFWA

In this study, the evaluation of the WRF-Chem model output was primarily qualitative. To enable a quantitative comparison, further investigations using reliable observational data are essential. Due to the unavailability of ground-based observational data in this region, comparing the model output with such data was not feasible. Therefore, the WRF-Chem model's dust surface concentration forecasts (36- to 60-h range) were compared with MERRA2 reanalysis data. Considering that on the one hand, the MERRA2 reanalysis data need to be validated and on the other hand, there was a significant difference between the concentration values obtained by the model and the reanalysis data, a quantitative comparison was not possible.

Data

Aerosol optical depth

Aerosol Optical Depth (AOD) measures how much aerosols in the atmosphere prevent light from passing through. Aerosols scatter and absorb sunlight, reducing visibility. For an observer on Earth, an AOD of less than 0.1 indicates a clear blue sky, bright sun, and maximum visibility. As AOD increases to 0.5, 1, or above 3, aerosols become so concentrated that the sun may be obscured. Since detecting aerosols over different types of land and ocean surfaces can be challenging, various algorithms have been developed to aid in identifying aerosols and calculating AOD. In this study, AOD data derived from a combination of the Dark Target (DT) and Deep Blue (DB) algorithms, using MODIS/TERRA data, were obtained from NASA's Worldview. This integrated DT/DB AOD layer offers a comprehensive view of AOD over both land and ocean surfaces. It combines three algorithms: two DT algorithms for retrieving aerosols over ocean surfaces (which appear dark at visible and longer wavelengths) and vegetated or soil-covered land (which appears dark at visible wavelengths), and a DB algorithm designed to retrieve aerosols over desert or arid regions (which appear bright at visible wavelengths). Depending on the surface characteristics of a specific location, the appropriate algorithm is applied. The sensor/algorithm resolution in Nadir is 10 km, the image resolution in Nadir is 2 km, and the data are available with daily temporal resolution.

GFS forecast data

The GFS forecast data used in this study are global data with a horizontal resolution of 0.25 degrees. These data are available from 0 to 240 h with a 3-h interval and from 240 to 384 h later in a 12-h interval. The model run 4 times a day at 00, 06, 12, and 18 UTC.

MERRA2 data

MERRA-2 is a reanalysis data product developed by NASA's Global Modeling and Assimilation Office (GMAO). It is currently produced using version 5.12.4 of the GMAO/GEOS-5 model. The data have an original spatial resolution of 0.5° latitude by 0.625° longitude, with 72 sigma/pressure hybrid vertical levels. MERRA-2 data are stored on the same vertical grid as the GEOS-5 forward processing (GEOS-FP) system, alongside Met MERRA field products. The GEOS-5 Forward Processing Atmospheric Data Assimilation System (ADAS) is based on an analysis developed in collaboration with NOAA's National Centers for Environmental Prediction (NCEP). This collaboration allows GMAO to incorporate advancements from NCEP and the Joint Center for Satellite Data Assimilation (JCSDA). The GEOS-5 Atmospheric General Circulation Model (AGCM) employs finite-volume dynamics [27], along with various physics packages [28]. These are integrated under the Earth System Modeling Framework (ESMF), which includes a Catchment Land Surface Model (CLSM), as described by [29].

Study area

Fig. 1 illustrates the study area, encompassing

the three northern provinces of Iran, Gilan, Mazandaran, and Golestan as well as the geographic locations of several meteorological stations within the region. These stations recorded weather codes related to dust during at least one of the three studied dust events. The study area lies between the southern shores of the Caspian Sea and the Alborz mountain range, making it the rainiest region in Iran, with substantial forest cover. However, in recent years, severe droughts have led to the formation of numerous dust sources around the area, which now significantly affect the region. Additionally, the intensity of non-local dust storms has increased to the extent that, despite the area's complex topography and its proximity to the Alborz mountains to the south and the Caspian Sea to the north, these storms have had a marked impact.

Results and discussion

The true color images of the MODIS/Terra satellite related to three dust events in the southern Caspian shores are shown in Fig. 2. On April 8, 2022 (Fig. 2A), the dust mass along with clouds is observed in a large part of the southern Caspian Sea and its southern and eastern coasts. On May 5, 2022 (Fig. 2B), there was dust in east of Iraq, west and northwest of Iran, the southern and eastern shores of the Caspian Sea, as well as its central regions. On this day, severe cloudiness is observed over Turkey, the western, northern and eastern coasts of the Caspian Sea. On May 24, there is dust in the northern Iraq, northwestern Iran, southern Caspian Sea and its southern and eastern coasts. On this day, the mass of clouds can be seen over Turkey, the western and northern coasts of the Caspian Sea.

Fig. 1. The study area and synoptic meteorological stations

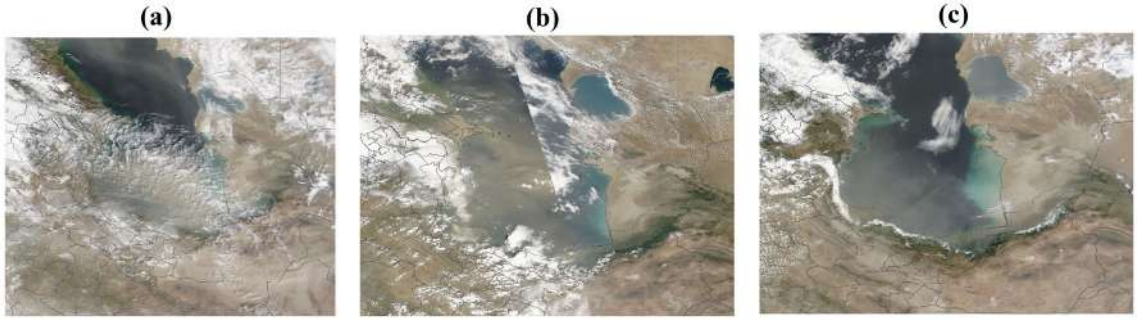

Fig. 2. True color image of MODIS/Terra satellite on a) April 8, b) May 5, c) May 24, 2022

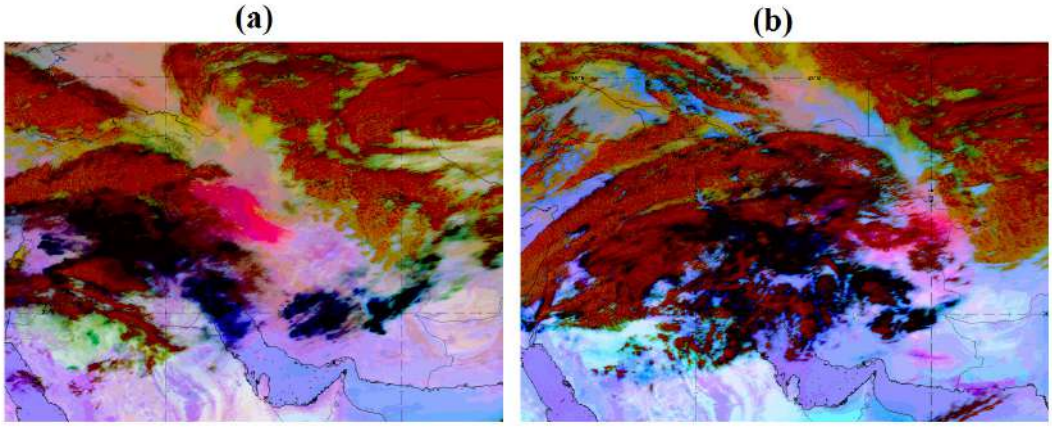

Fig. 3. Dust RGB product of MSG satellite at a) 00, b) 12 UTC on April 8, 2022

Case study 20220408

Data from synoptic meteorological stations

The data of the present weather code, horizontal visibility and wind speed and direction in the stations of the north of Iran, which reported the code related to dust on April 8, 2022, along with the station specifications, are shown in the Table 1 in the appendix given on this day. Dust was reported in four stations located in Gilan province and two stations in Mazandaran province at different times of the day. Minimum visibility of 800 m at 15 UTC was recorded at Alasht, located in the east of Mazandaran.

RGB dust product of the MSG satellite

Fig. 3 shows the RGB dust product of the MSG satellite at different hours on April 8, 2022. At 00 UTC, a heavy dust mass is observed in northwest of Iran and southwestern shores of the Caspian Sea. The presence of cloud mass in a large part of the region prevented the dust detection. However, in areas of Iraq, southeastern Syria and northeastern Arabia, as well as a large part of Iran, dust is observed around the clouds. At 12 UTC, the southern shores of the Caspian Sea were covered by clouds, but dust is still observed around the cloud mass.

CALIPSO products

Fig. 4 shows CALIPSO satellite products in a part of its path that passes through northeast of Iran, the eastern shores of the Caspian and its northern regions at around 10 UTC on April 8, 2022. The Total Attenuated Backscatter (TAB) values show that there was aerosol in a large part of the region near the ground to a height of about 6 km. In addition, the high values of TAB over the Caspian Sea at an altitude of about 10 km are related to the clouds in this area. The Vertical Feature Mask (VFM) coverage product also shows the presence of aerosols in the region and even below and among the clouds. According to the product type (Fig. 4d), in almost all regions the aerosols were of the dust type, except the area of the Arabian Sea and the Oman Sea, particles were of the marine dust type.

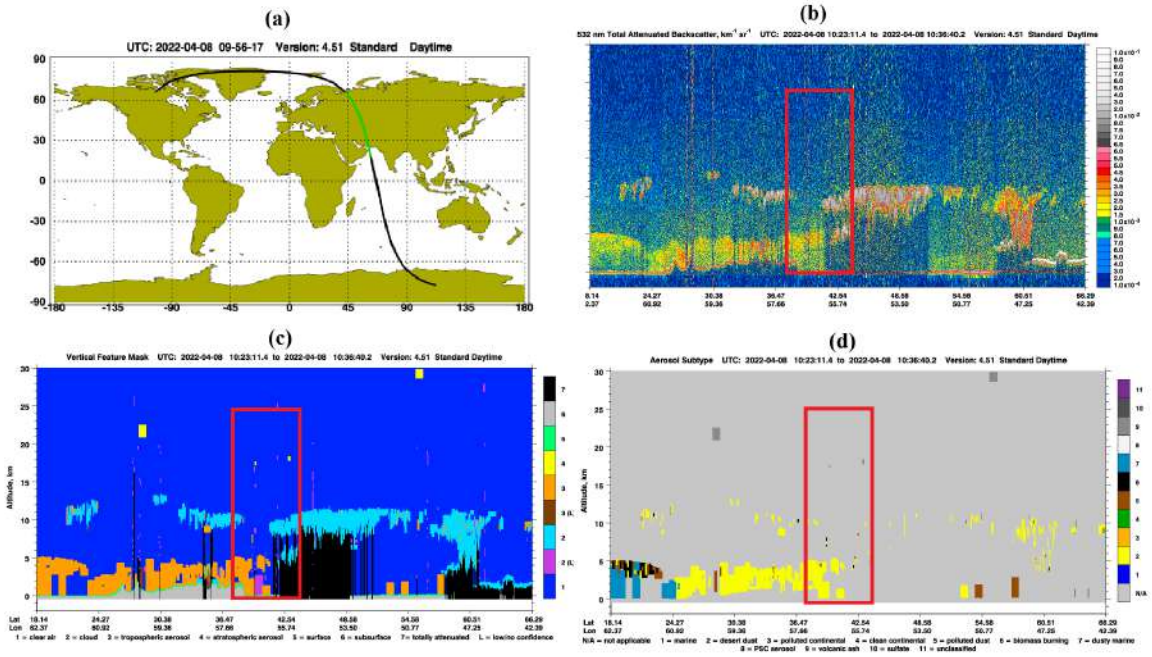

Fig. 4. a) CALIPSO satellite trajectory, b) total attenuated backscatter, c) vertical feature mask, d) aerosol type at 10:23UTC on April 8, 2022

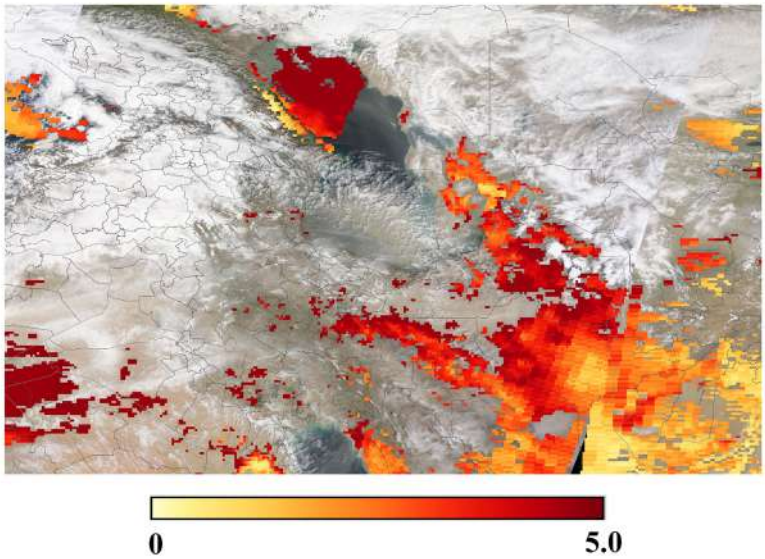

Fig. 5. The AOD product of MODIS/Terra satellite on April 8, 2022

The AOD product of MODIS/Terra satellite

Fig. 5 shows the AOD product of the MODIS/Terra satellite on April 8, 2022. On this day, due to cloud cover, there was no data in a large part of the area. However, AOD values were significant in western Iraq, central areas of Iran, eastern shores of the Caspian Sea located in western Turkmenistan, northern Caspian Sea and some small areas of the southern Caspian shores. Another factor that causes the increase of AOD on the sea and coastal areas is the entry of sea salt into the atmosphere. The very high values of AOD in a part of the region and the aerosol product from the CALIPSO satellite show that the aerosols are of the dust type.

Synoptic analysis

At 06 UTC on April 8, 2022 in the surface map, a low-pressure center was located over the Black Sea and extends to the west of the Caspian Sea. High pressure spread over Russia and continued to the east of the Caspian Sea. On the Caspian Sea, the extreme pressure gradient caused strong south and southeasterly winds to blow in its northern half. The strong southerly winds over the west of Iraq caused dust to be emitted from susceptible areas to the north-east of Iraq, and in that region the westerly winds directed the dust to the north-west of Iran and the southern shores of the Caspian Sea. A low pressure was over the central regions of Iran (south of Semnan and north of Isfahan), where the strong westerly winds in the south of the low pressure caused dust emission from this region and its transfer to the northeast of Iran (Fig. 6a).

At the level of 850 hPa, above the low pressure located on the east of the Black Sea, a deep trough can be seen that extended to the west of Afghanistan. This trough had an axis in the northwest-southeast direction (negative tilt), which was due to the faster movement of its southern part. The presence of surface low pressures on the eastern side of trough in the central regions of Iran and Afghanistan, was also the other factor that caused negative tilt. Another factor was the presence of severe baroclinity in the southern parts of the trough, which was well noticeable in the eastern regions of the miner trough. The negative tilt of the trough causes severe storms, heavy rains and bad weather. In this case, it caused strong winds and dust emission in the central regions of Iran. There was a miner trough above the surface low pressure over the central regions of Iran and a strong ridge above the Siberian high pressure. Strong westerly wind is observed in the central regions of Iran. The change of wind direction to the southerly and southeasterly winds in the eastern part of the low pressure caused the dust transfer from these areas to the North Khorasan, Golestan and East of Mazandaran (Fig. 6b). For a more detailed analysis of the wind speed, a map of the streamlines at 850hPa level is shown (Fig. 6c). In the northern regions of Iraq, southwesterly and westerly currents are observed, which caused dust to be transferred to the border areas of Iran. In the west and north-west of Iran, strong westerly currents caused dust to be transported to the southern shores of the Caspian. The transfer of dust from the central regions to the north of Iran is also confirmed in this pattern. A positive vorticity can be seen in a region located in the north and northeast of Iran, exactly in the area of miner trough in Fig. 6b. In addition, in the northern part of the western Caspian Sea, a positive vorticity center is observed. At the level of 500hPa (Fig. 6d), a trough was stretched from the east of the Black Sea to the southeast of Iran, and a miner trough can be seen in the southern part of it, which is the place of dust emission.

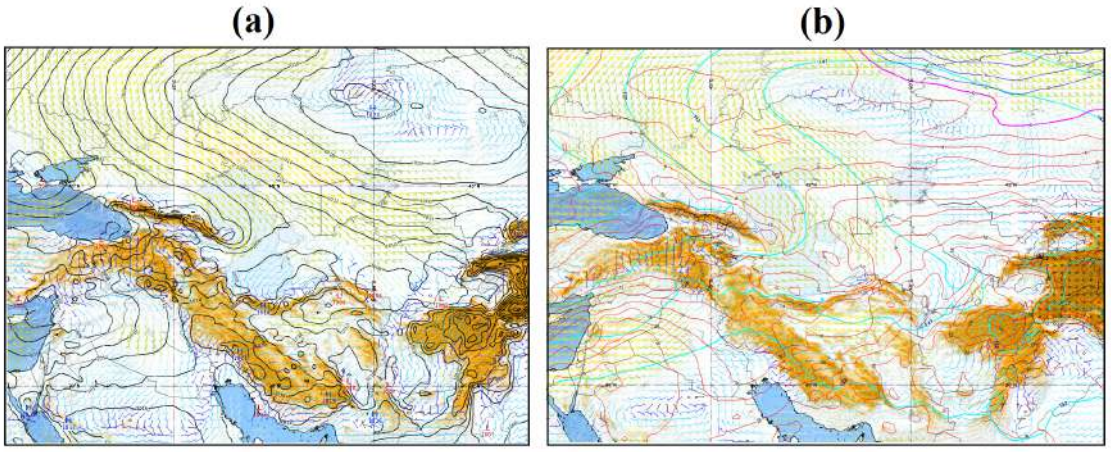

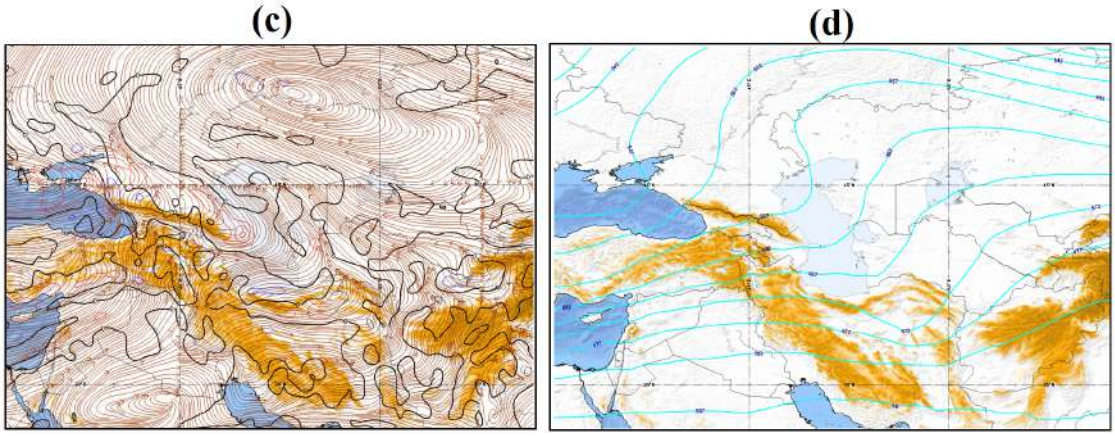

Fig. 6. a) Mean sea level pressure and wind at 950hPa, b) wind, geopotential height and temperature at 850hPa, c) stream lines and relative humidity at 850hPa, d) geopotential height at 500hPa at 06 UTC on April 8, 2022

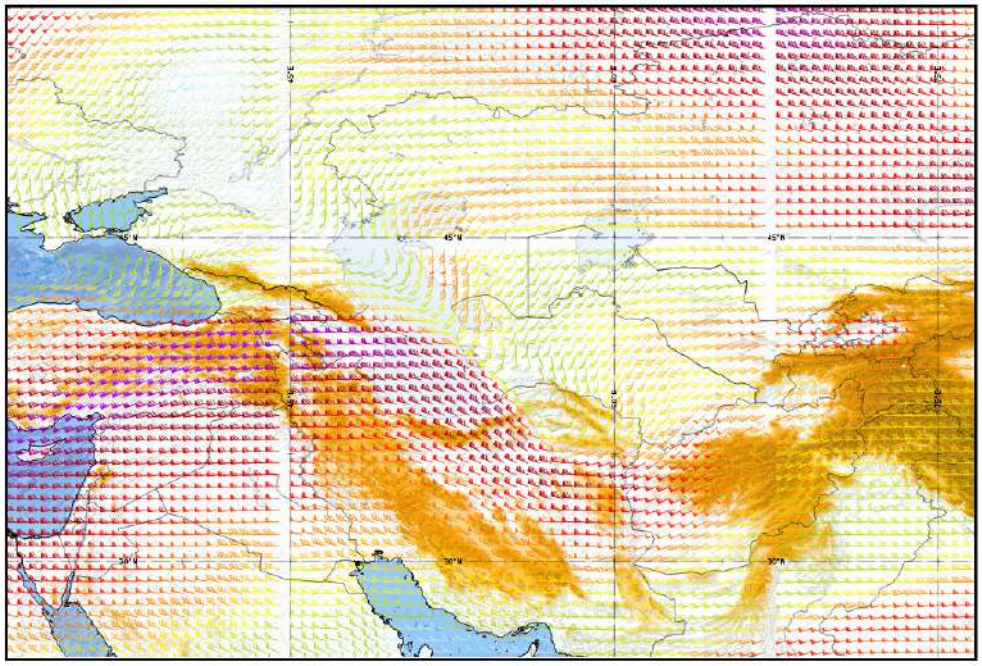

Fig. 7. Wind vector at the level of 300hPa at 06 UTC on April 8, 2022

The wind of 300 hPa in the Fig. 7 shows that the core of the jet stream with a speed of more than 55 m/s was located in the east of Turkey, Azerbaijan and the west of the Caspian Sea. The jet stream shows the strengthening of instability in the atmospheric lower levels [30]. The wind speed was lower on the northern areas of 850 hPa trough (east and northeast of the Black Sea), which was accompanied by the jet stream in the northern part. However, in the southern part of the trough, which was separated from the northern part (central regions of Iran); the wind speed was higher. These results are consistent with the results of [19], which stated that a positive orbital and meridional wind component in the lower levels of troposphere is among the necessary conditions for dust transport from the source to a long distance in the north of Iran. In addition, the presence of positive vorticity at 500 hPa level and the accompanying jet stream at 300 hPa level, made it possible for dust particles to climb and pass over the mountain heights.

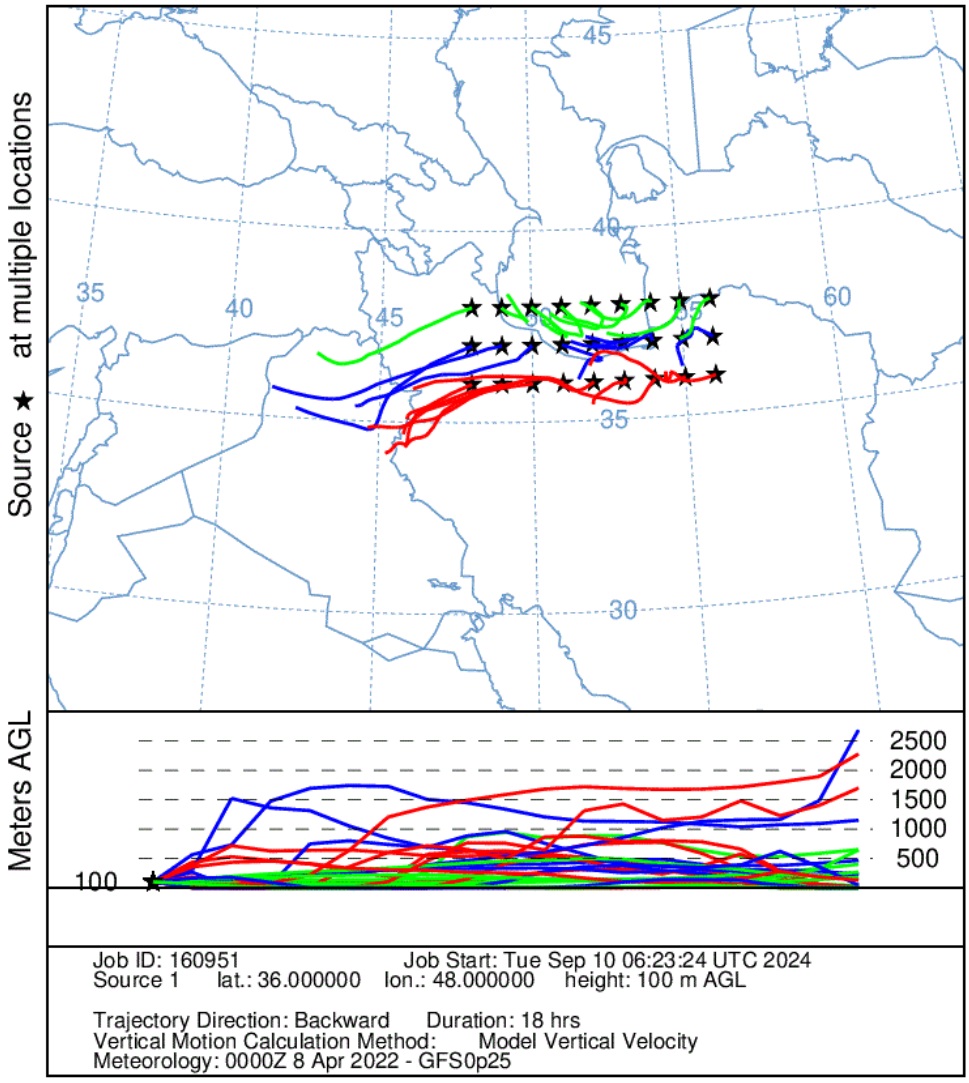

Fig. 8. The backward trajectory of HYSPLIT model at 100 m height for 18 h, at 12 UTC, on April 8, 2022

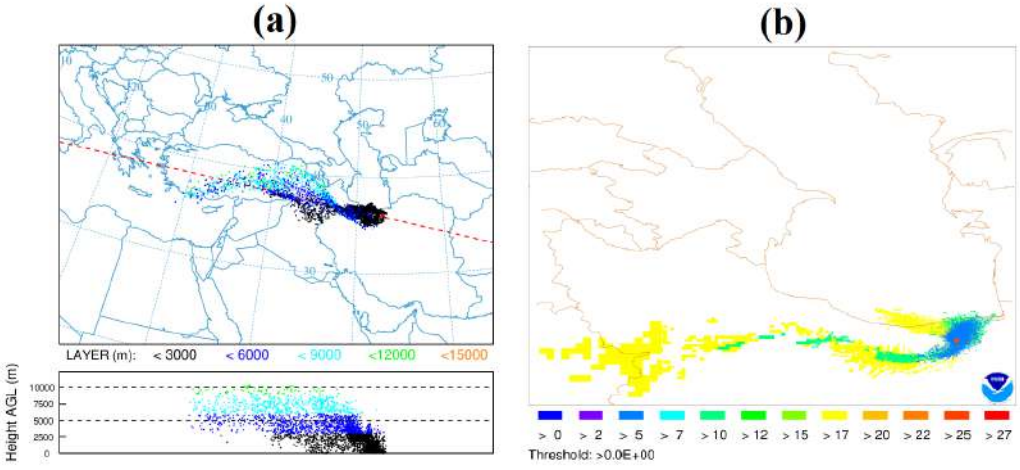

Fig. 9. a) The plume arrival (hours) from the initial time, b) particle position (m) of the HYSPLIT dispersion model for the initial time of 12 UTC April 8, 2022

HYSPLIT model output

Fig. 8 shows the output of the HYSPLIT trajectory model. The model was implemented in the form of a matrix with the backward method for 18 h at an altitude of 100 m. the model was started at 12 UTC on April 8, 2022 in the southern shores of the Caspian Sea. According to the results, a major part of the dust from the northern regions of Iraq entered the northwestern regions of Iran through the westerly and southwesterly currents and after that, the dust entered the Caspian Sea southern shores with the westerly currents. Of course, the presence of southerly and south-westerly currents in Mazandaran province caused the dust to be transferred from the central regions of the country to this part as well, in such a way that the lowest amount of horizontal visibility was reported in the eastern half of Mazandaran province.

Fig. 9 shows the output of the HYSPLIT dispersion model for a point located in the area of Alasht station in the eastern half of Mazandaran at 12 UTC on April 8. The vertical cross-section of the particle position shows that most of the particles that are observed at an altitude of less than 5 km, were located in northern Iraq, northwestern Iran, and finally on the southern shores of the Caspian Sea. The particles that are observed at a height between 6 and 9 km, which could act as condensation nuclei in clouds, spread in the northern Mediterranean, Turkey, northwestern Iran, and finally in the Caspian Sea southern shores. In this figure, the channelized area of the particles marked by a red rectangle (Manjil area) where the dust particles passed through the Alborz mountain range and then dispersed on the southern shores of the Caspian Sea, which has a lower height [12]. Some studies showed that dust particles rising to the mid-levels of the atmosphere in the source region passed over the Zagros Mountains and entered the Caspian Sea through the Manjil Valley [11, 16]. In this study, the vertical profile of dust concentration from the WRF-Chem model output revealed the ascent of dust particles up to 600 hPa near the dust source, followed by their movement through mountainous areas.

The arrival time map also shows that the particles that entered the starting point of the model entered this region from the north of Iraq about 17 h ago.

Comparison of WRF-Chem model output and MERRA2 reanalysis data

The dust surface concentration and wind velocity at the 10-m output of the WRF-Chem model, which was implemented from 12 UTC on April 6 as the initial time, and the dust surface concentration from MERRA2 reanalysis data for 00 and 12 UTC on April 8 is shown in Fig. 10. At 00 UTC in the output of the WRF-Chem model, the dust affected a large part of Iraq, west, north-west, north and center of Iran, as well as the eastern shores of the Caspian Sea located in the west of Turkmenistan. The change of wind direction in western Iraq shows that the model correctly predicted the position of the cold front in western Iraq and the pre-frontal dust. In the MERRA2 reanalysis data, dust concentration is highest in the eastern half of Iraq, northwestern and central Iran, and the southern and eastern coasts of the Caspian. In this time, the two dust patterns are very similar. The most difference is observed in the Turkmenistan and northeastern Iran, where the model did not predict the dust over this region well.

At 12 UTC, the WRF-Chem model shows that dust entered the southern regions of the Caspian Sea. On the other hand, the wind speed and dust concentration in the eastern Syria and western Iraq increased sharply. In the data of MERRA2, the concentration of dust increased in the east of Syria and western half of Iraq, as well as the southern border of the Iran-Iraq and the western and southwestern regions of Iran. On the southern shores of the Caspian Sea, the highest dust concentration is observed in southeast and the border of Mazandaran and Golestan provinces. At this hour, the WRF-Chem model overestimated the dust concentration in the western half of Iraq and underestimated in the southeast coast of the Caspian Sea.

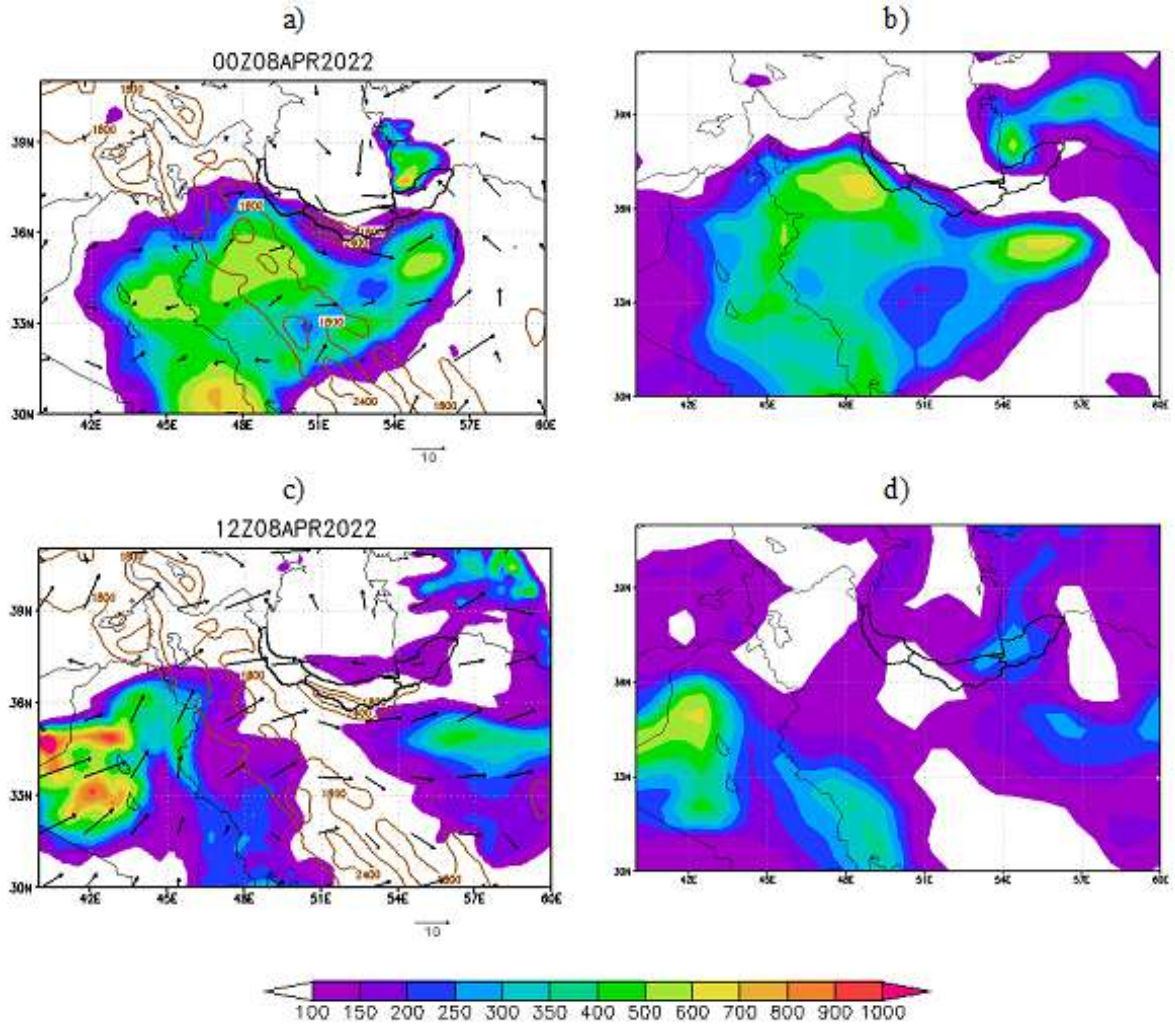

Fig. 10. The dust surface concentration (ug/m3) and 10-m wind (m/s) from the WRF-Chem model output, which was implemented from 12 UTC on April 6 as the initial time (a, c) and the dust surface concentration from MERRA2 reanalysis data. (b, d) for 00 and 12 UTC on April 8, 2022

Case study 20220505

Data from synoptic meteorological stations

The Table 2 shows the quantities of the present weather code, horizontal visibility and wind direction and speed in the stations in the north of the Iran that reported the weather code related to dust on May 5. On this day, dust was observed only in Gilan province, located in the southwest of the Caspian Sea, between 9 and 18 UTC. Horizontal visibility of 5 to 6 km was reported in Jirandeh and Manjil stations. The slight decrease in horizontal visibility suggests that dust in the region often stays in the upper atmospheric levels [12].

Table 2. The present weather code data, horizontal visibility and wind speed and direction in stations located in the northern provinces of Iran on the date of 20220408

Station	Province	Lat	Lon	Elevation (m)	date	Weather code	Visibility (m)	Wind speed (m/s)	Wind direction
Jirandeh	Gilan	36.71	49.8	1581.4	4/8/2022 3:00	7	2000	2	260
Jirandeh	Gilan	36.71	49.8	1581.4	4/8/2022 6:00	7	2000	2	210
Jirandeh	Gilan	36.71	49.8	1581.4	4/8/2022 9:00	7	2000	2	210
Manjil	Gilan	36.73	49.41	338.3	4/8/2022 9:00	6	6000	2	210
Astara	Gilan	38.37	48.85	-21.1	4/8/2022 9:00	6	5000	5	130
Talesh	Gilan	37.84	48.9	7	4/8/2022 9:00	6	7000	2	130
Baladeh	Mazandaran	36.2	51.8	2120	4/8/2022 9:00	9	9000	6	180
Jirandeh	Gilan	36.71	49.8	1581.4	4/8/2022 12:00	7	2000	4	110
Manjil	Gilan	36.73	49.41	338.3	4/8/2022 12:00	6	3000	2	340
Astara	Gilan	38.37	48.85	-21.1	4/8/2022 12:00	6	4000	2	90
Talesh	Gilan	37.84	48.9	7	4/8/2022 12:00	6	5000	2	110
Jirandeh	Gilan	36.71	49.8	1581.4	4/8/2022 15:00	7	2000	6	150
Manjil	Gilan	36.73	49.41	338.3	4/8/2022 15:00	6	3000	1	340
Astara	Gilan	38.37	48.85	-21.1	4/8/2022 15:00	6	5000	2	160
Talesh	Gilan	37.84	48.9	7	4/8/2022 15:00	6	5000	2	100
Alasht	Mazandaran	36.07	52.84	1805	4/8/2022 15:00	6	800	0	0
Manjil	Gilan	36.73	49.41	338.3	4/8/2022 18:00	6	4000	1	80
Manjil	Gilan	36.73	49.41	338.3	4/8/2022 21:00	6	10000	2	60

RGB dust product of the MSG satellite

Fig. 11a,b shows the dust RGB product of MSG satellite at different hours of May 5, 2022. At 00 UTC, the central and northeastern regions of Iraq and parts of northwestern Iran were covered by heavy dust. At 12 UTC, dust entered a wide part of the Caspian Sea. At this time, there was still dust in a large part of Iraq, northeastern Saudi Arabia, and western and northwestern Iran.

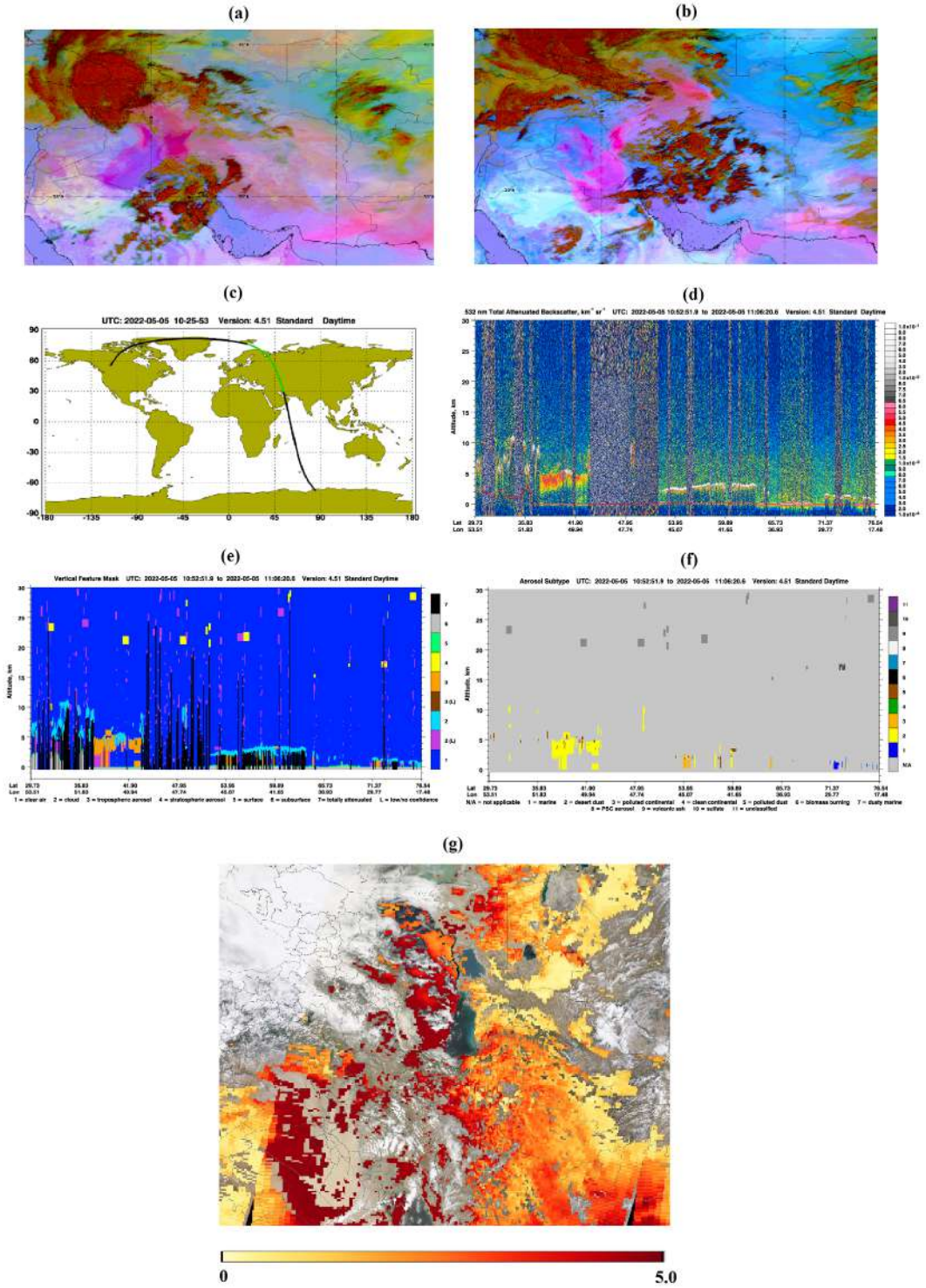

Fig. 11. Dust RGB product of MSG satellite at a) 00, b) 12UTC on May 5, 2022, c) CALIPSO satellite trajectory, d) total attenuated backscatter, e) vertical feature mask, f) types of aerosols at 10:52UTC on May 5, 2022, g) The AOD product of the MODIS/Terra satellite on May 5, 2022

CALIPSO products

CALIPSO products at around 11 UTC on May 5, 2022 are shown in Fig. 11c-f. At this time, the CALIPSO satellite passed the central part of the southern shores of the Caspian Sea to its northeast. In this area, the presence of aerosols can be seen near the surface to a height of about 5 km. In some parts, mid-level clouds were among the aerosols at a height of about 4 km. The type of aerosols shows that in general, they were of the dust type in this area.

The AOD product of MODIS/Terra satellite

The AOD data of the MODIS/Terra satellite on May 5, 2022 is shown in Fig. 11g. On this day, the highest AOD values were over Iraq, the southwestern and northwestern regions of Iran, the Caspian Sea, and its southwestern coasts. AOD values were also significant in the central and eastern regions of Iran and the eastern and southeastern coasts of the Caspian Sea.

Synoptic analysis

At 12 UTC on May 5, 2022 a low-pressure center can be seen in the southeast of Iraq and southwest of Iran, whose cold front was located in the east and southeast of Iraq. The dust mass in the dust RGB images over these areas was the prefrontal dust that observed behind the cold front. Another low pressure was in the northwest of Iran. In the southern part of it, strong southwesterly winds caused the dust emission from the northeast of Iraq to the northwest of Iran and the southern shores of the Caspian Sea. A weak high pressure closed over Gilan province. The third low pressure was in the border region of Iran and Turkmenistan. In the western part of this low-pressure, a dust mass can be seen in the satellite images. Due to the northeasterly and northerly winds blowing over the east and southeast of the Caspian Sea, the dust emitted from the west of Turkmenistan entered the southern parts of the Caspian Sea and its southeastern coasts (Golestan province and east of Mazandaran). The increase in wind speed due to the increase in the pressure gradient on the desert parts of the east of the Caspian Sea leads to the formation of northeasterly currents and the transport of dust towards the southern shores of the Caspian Sea [15]. Another low-pressure center formed over the central regions of Iran, which caused dust emission from these regions and transferred to the northeast of Iran. Due to the cloud cover in the RGB images, the dust in this area is not well visible (The figure is not shown).

At the level of 850hPa, the low geopotential height covered east of the Black Sea, the Caspian Sea, the northern half of Iran, northern Iraq, and eastern Turkey. There was a low geopotential height center in the northwest of Iran, and another was located above the low pressure in the central regions of Iran. In the eastern regions of Iraq, at the location of the cold front, baroclinity and cold air advection is seen. The north and northwesterly winds caused the transfer of dust from the northwest of Iraq to the southeast of Iran. Dust was transported from southeastern Iraq by southerly and southwesterly winds ahead of the cold front, moving toward northwestern Iran and the southwestern coasts of the Caspian Sea. One of the atmospheric factors that can cause dust is the existence of atmospheric fronts [31].

The westerly and northwesterly winds blowing over Iraq in the map of 850hPa streamlines, transferred the dust to the west and south-west of Iran. On the other hand, the southwesterly winds in the western Iran carried the dust to the northwest regions of Iran and southwestern Caspian shores. At the level of 500hPa, the trough extended from the Black Sea to the south-west of Iran. A miner trough is seen on the east and southeast of Iraq and another on the east of the Caspian Sea.

The dust was located in front of the trough axis; and penetrated to the upper levels of the atmosphere because of the upward motions and entered the southern shores of the Caspian Sea by passing through the topography of the area.

HYSPLIT model output

Fig. 12a shows the output of the HYSPLIT trajectory model for 12 UTC on May 5, 2022, using the backward method at an altitude of 100 m for 28 h. The trajectories indicate that in the western part of the southern shores of the Caspian Sea, particles originated from western and southern Iraq, while in the northern part of the eastern shores, they came from eastern Turkmenistan, and in the southern part, from central Iran. In this study, the dust-carrying currents toward the southern Caspian Sea followed various directions and passed through different paths. In the simulation study of dust emitted from Turkmenistan to the southern shore of the Caspian Sea introduced an active source of dust source in the eastern parts of the Caspian Sea, on the desert areas of the Turkmenistan and Qaraqom deserts [15].

The output of the HYSPLIT dispersion model for a point located on the southeastern coast of the Caspian Sea at 12 UTC on May 5, 2022, is shown in Fig. 12b. The vertical cross section of the particle position shows that most of the particles were located at a height of less than 4 km and entered this region from northern Saudi Arabia, western and central Iraq, and southwestern and central Iran. There were some particles at a higher height (between 4 and 6 km), that were located in the north of Saudi Arabia and west of Zagros. In addition, some particles from northeastern Iran and the border region with Turkmenistan affected this region. The arrival time map shows that the particles were in northern Saudi Arabia and Iraq about 22 h ago. In southwest and west of Iran, particles were located between 16 and 10 h ago. About 4 h before the start time, the particles were over Alborz. The particles that came from the southwest of Turkmenistan were also present there about 22 h ago, despite the shorter distance, which shows that they were transported to the region at a slower speed.

Comparison of WRF-Chem model output and MERRA2 reanalysis data

The dust surface concentration and 10-m wind velocity output of the WRF-Chem model, which was implemented from 12 UTC on May 3, 2022 as the initial time, and the dust surface concentration from MERRA2 reanalysis data for 00 and 12 UTC on the 5th May 2022 is shown in Fig. 12c,d. At 00 UTC in the output of the WRF-Chem model, the highest concentration of dust observed in the central regions of Iraq. All over the country of Iraq and the western and northwestern regions of Iran were affected by dust. Northwesterly winds in the central regions of Iraq caused the dust to be transported to the southeast of Iraq, and southwesterly winds in this region caused particles to be transported to the northwest of Iran. Change of wind direction shows that the model was able to predict the presence of a cold and dusty front. In MERRA2 data, although the western half of Iran affected by dust, the highest concentration of dust was over Iraq. The two dust patterns in this time are very similar to each other.

At 12:00 UTC, according to the WRF-Chem model output, strong southerly winds in southwest Iran greatly increased the dust concentration in this region. The dust concentration over Iraq decreased. In the MERRA2 data, the concentration of dust increased in the west of Iran, and the provinces of Gilan and Mazandaran were affected by dust. At this hour, there was a significant difference between the two patterns of dust concentration. The WRF-Chem model did not show any dust over the northwestern regions of Iran and the southern shores of the Caspian Sea, unlike MERRA2.

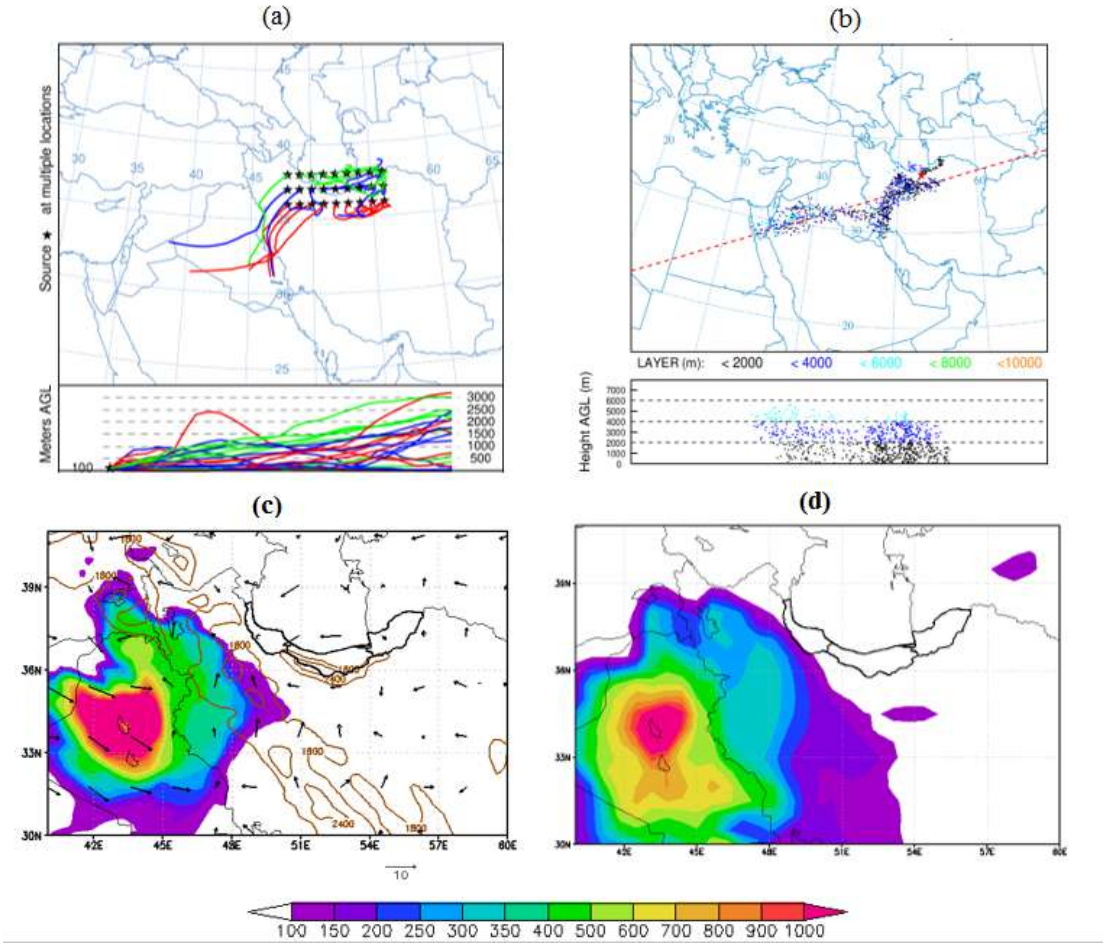

Fig. 12. The backward trajectory of HYSPLIT model at 100 m height for 18 h, at 12 UTC on May 5, 2022, b) The plume arrival (hours) from the initial time of the HYSPLIT dispersion model for the initial time of 12 UTC May 5, 2022, c) The dust surface concentration and 10-m wind from the WRF-Chem model output, which was implemented from 12 UTC on April 6 as the initial time, d) the dust surface concentration from MERRA2 reanalysis data for 00:00 UTC on May 5, 2022

Case study 20220524

Data from synoptic meteorological stations

The present weather code, horizontal visibility, wind speed and direction data in the stations located in the north of Iran that reported the code related to dust on May 24, 2022, along with the station specifications is shown in the Table 3. In this case study dust was reported in a large number of stations located in Gilan, Mazandaran and Golestan provinces at different hours. The minimum visibility was reported from Jirande station located in Gilan province at 9, 12 and 15 UTC. Table 4 shows the present weather code data, horizontal visibility and wind speed and direction in stations located in the northern provinces of Iran on the date of 20220524

RGB dust product of the MSG satellite

Fig. 13a,b shows the dust RGB product of the MSG satellite at different hours on May 24, 2022. At 00 UTC, heavy dust is observed in eastern Iraq, western and northwestern Iran, western Caspian Sea and its southwestern coasts. At 12 UTC, the intensity of dust increased in the southwest of the Caspian Sea and the coasts of this region. At this time, the whole northern half of Iran was affected by dust.

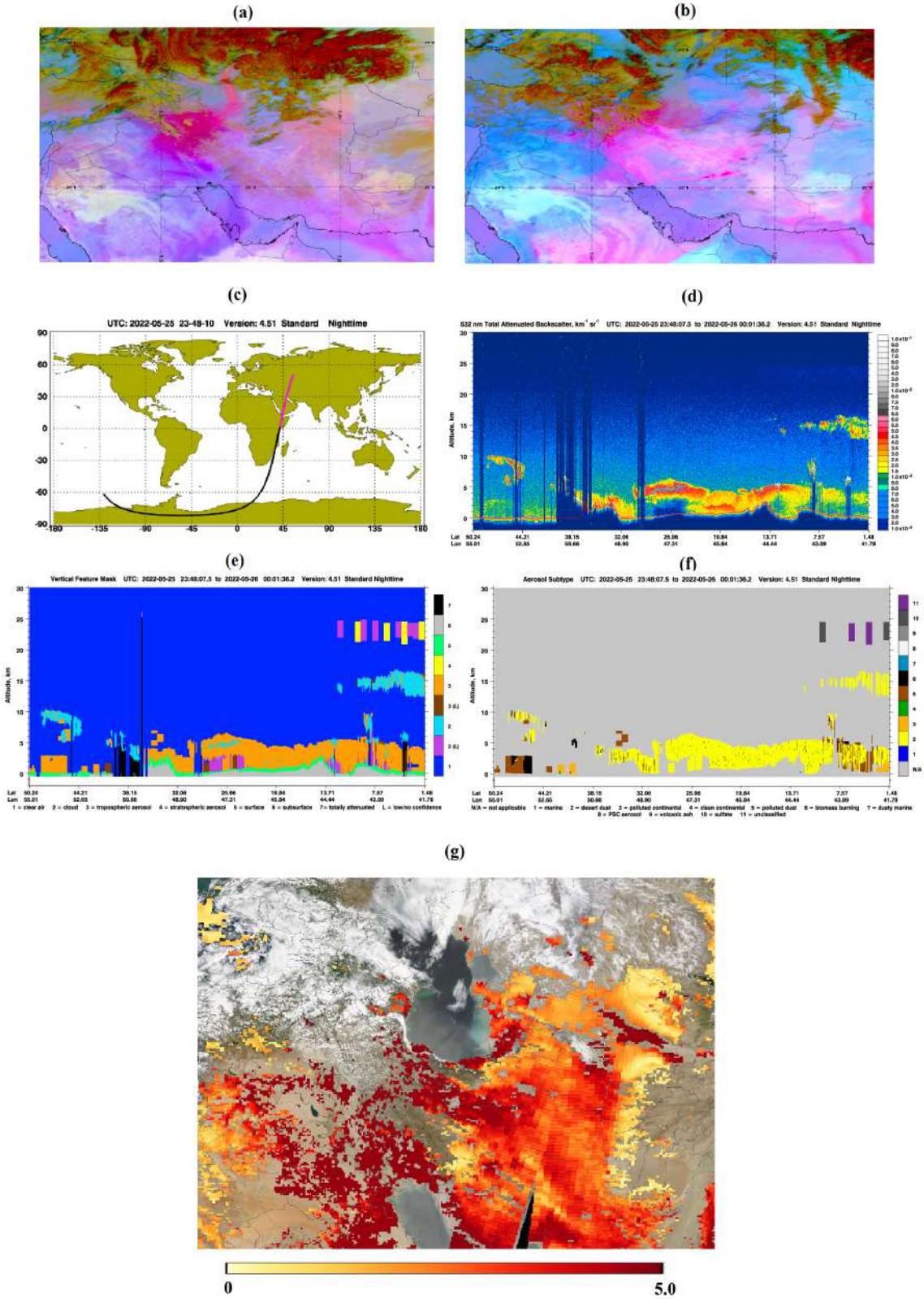

Fig. 13. Dust RGB product of MSG satellite at a) 00, b) 12UTC on May 24, 2022, c) CALIPSO satellite trajectory, d) total attenuated backscatter, e) vertical feature mask, f) types of aerosols at around 23 UTC on May 25, 2022, g) The AOD product of the MODIS/Terra satellite on May 24, 2022

Table 3. The present weather code, horizontal visibility and wind speed and direction data in stations located in the northern provinces of Iran on the date of 20220505

Station	Province	Lat	Lon	Elevation (m)	date	Weather code	Visibility (m)	Wind speed (m./s)	Wind direction
Jirandeh	Gilan	36.71	49.8	1581.4	5/5/2022 9:00	6	8000	10	160
Jirandeh	Gilan	36.71	49.8	1581.4	5/5/2022 12:00	6	5000	10	210
Manjil	Gilan	36.73	49.41	338.3	5/5/2022 12:00	6	6000	3	350
Jirandeh	Gilan	36.71	49.8	1581.4	5/5/2022 15:00	6	5000	7	230
Manjil	Gilan	36.73	49.41	338.3	5/5/2022 15:00	6	8000	11	360
Manjil	Gilan	36.73	49.41	338.3	5/5/2022 18:00	6	8000	4	20

Table 4. The present weather code data, horizontal visibility and wind speed and direction in stations located in the northern provinces of Iran on the date of 20220524

Station	Province	Lat	Lon	Elevation (m)	date	Weather code	Visibility (m)	Wind speed (m/s)	Wind direction
Jirandeh	Gilan	36.71	49.8	1581.4	5/24/2022 3:00	6	2000	1	320
Inchehborun	Golestan	37.45	54.72	7	5/24/2022 3:00	7	6000	12	210
Maravehtappeh	Golestan	37.8	55.94	460	5/24/2022 3:00	7	8000	21	180
Astara	Gilan	38.37	48.85	-21.1	5/24/2022 3:00	6	5000	1	290
Jirandeh	Gilan	36.71	49.8	1581.4	5/24/2022 6:00	6	2000	1	190
Manjil	Gilan	36.73	49.41	338.3	5/24/2022 6:00	6	7000	3	350
Maravehtappeh	Golestan	37.8	55.94	460	5/24/2022 6:00	7	8000	15	190

Table 4. Continued

Station	Province	Lat	Lon	Elevation (m)	date	Weather code	Visibility (m)	Wind speed (m/s)	Wind direction
Talesh	Gilan	37.84	48.9	7	5/24/2022 6:00	6	5000	2	110
Astara	Gilan	38.37	48.85	-21.1	5/24/2022 6:00	6	4000	3	120
Jirandeh	Gilan	36.71	49.8	1581.4	5/24/2022 9:00	6	1500	2	220
Manjil	Gilan	36.73	49.41	338.3	5/24/2022 9:00	6	7000	8	360
Talesh	Gilan	37.84	48.9	7	5/24/2022 9:00	6	5000	3	140
Maravehtappeh	Golestan	37.8	55.94	460	5/24/2022 9:00	7	7000	10	210
Astara	Gilan	38.37	48.85	-21.1	5/24/2022 9:00	6	3000	3	140
Jirandeh	Gilan	36.71	49.8	1581.4	5/24/2022 12:00	6	1500	4	230
Manjil	Gilan	36.73	49.41	338.3	5/24/2022 12:00	6	8000	15	360
Maravehtappeh	Golestan	37.8	55.94	460	5/24/2022 12:00	7	7000	6	220
Alasht	Mazandaran	36.07	52.84	1805	5/24/2022 12:00	6	7000	3	120

CALIPSO products

CALIPSO satellite products at around 23 UTC on May 25, 2022 are shown in Fig. 13c-f. In a part of the satellite path that passed from the southeast to the northwest of the Caspian Sea, aerosols are observed near the surface to a height of about 4 km. The type of aerosols shows that on the southwestern coast of the Caspian Sea, at an altitude between 2 and 5 km, most of the aerosols were of the dust type.

The AOD product of MODIS/Terra satellite

Fig. 13g shows the AOD values of the MODIS/Terra satellite on May 24, 2022. The highest AOD values on this day is observed in a large part of Iraq, west, south-west and center of Iran, as well as the southern shores of the Caspian Sea. In general, the amount of AOD was significant throughout Iran.

Synoptic analysis

At 12 UTC, 24 May 2022 a low pressure was in northern Iraq and high pressure in the east of the Black Sea extended to the west of the Caspian Sea. The pressure gradient caused by these two systems blew strong westerly winds in the east and north of Iraq and emitted dust from these areas to the north-west of Iran, and then the southwesterly and westerly winds directed the dust to the south-west coasts of the Caspian Sea (is not shown in Figure).

At the level of 850hPa, a deep trough entered the Caspian Sea. A cutoff low formed in the north-west of Iran, which trough has northern Iraq and eastern Syria. Cold advection can be clearly seen over the Caspian Sea. In the 850hPa streamlines, strong westerly currents over northern Iraq and southwesterly currents in northwestern Iran, caused dust to be transported to southwestern Caspian Sea. At 500hPa level, a low geopotential height was over Russia and penetrated to northern Saudi Arabia. whose southern part extended from the Black Sea to the northern Saudi Arabia. In general, Iraq, the western regions of Iran and the Caspian Sea were located in front of the trough axis.

HYSPLIT model output

Fig. 14a shows the output of the HYSPLIT trajectory model, which was implemented in the matrix form and in the backward method for the southern shores of the Caspian Sea for 24 h at an altitude of 100 m. In the western half of the region, the presence of westerly currents transferred dust from Iraq. In the northern east part, northerly currents were dominant, and in the southern part, southwesterly currents caused the dust to be transferred from the central regions of Iran to the study area.

Fig. 14b shows the HYSPLIT dispersion model output for a point located in the eastern Mazandaran at 12 UTC on May 24. The vertical cross-section of the particle position shows that most of the particles located at a height of less than 2 km entered this region from the Caspian Sea. The particles that were between 2 and 4 km height were located in the west of this area. The arrival time map also shows that some of the particles in this area were in the eastern Iraq and western Iran about 17 h ago.

Comparison of WRF-Chem model output and MERRA2 reanalysis data

The dust surface concentration and 10m-wind velocity output of the WRF-Chem model, which was implemented from 12 UTC on May 22, 2022 as the initial time, and the dust surface concentration from MERRA2 reanalysis data for 00, 06, 12 and 18 UTC May 24, 2022 are shown in Fig. 14c,d. At 00 UTC, based on the WRF-Chem model output, the highest dust concentration was in the north and south-east of Iraq and west of Iran. Because of westerly winds blowing over northern Iraq and northwestern Iran, dust entered the western half of the southern shores of the Caspian Sea. Also, dust is observed over the eastern Caspian Sea shores in the west of Turkmenistan. In MERRA2 data, dust concentration was significant in the northern Iraq, western Iran and western Turkmenistan and observed in Gilan and Mazandaran provinces. At this hour, the WRF-Chem model predicted more dust concentration values over Iran, Iraq, and less in the east of the Caspian Sea.

At 12 UTC, in the output of the WRF-Chem model, the dust concentration decreased in the northwest of Iran, and dust is observed only in the south of Mazandaran and the north of Golestan in the north of the country. According to the MERRA2 reanalysis data, the concentration of dust increased in the southeast of Iraq and southwest of Iran. The southern coast of the Caspian Sea was covered by dust. At this hour, the WRF-Chem model showed dust over wider parts of the central regions of Iran.

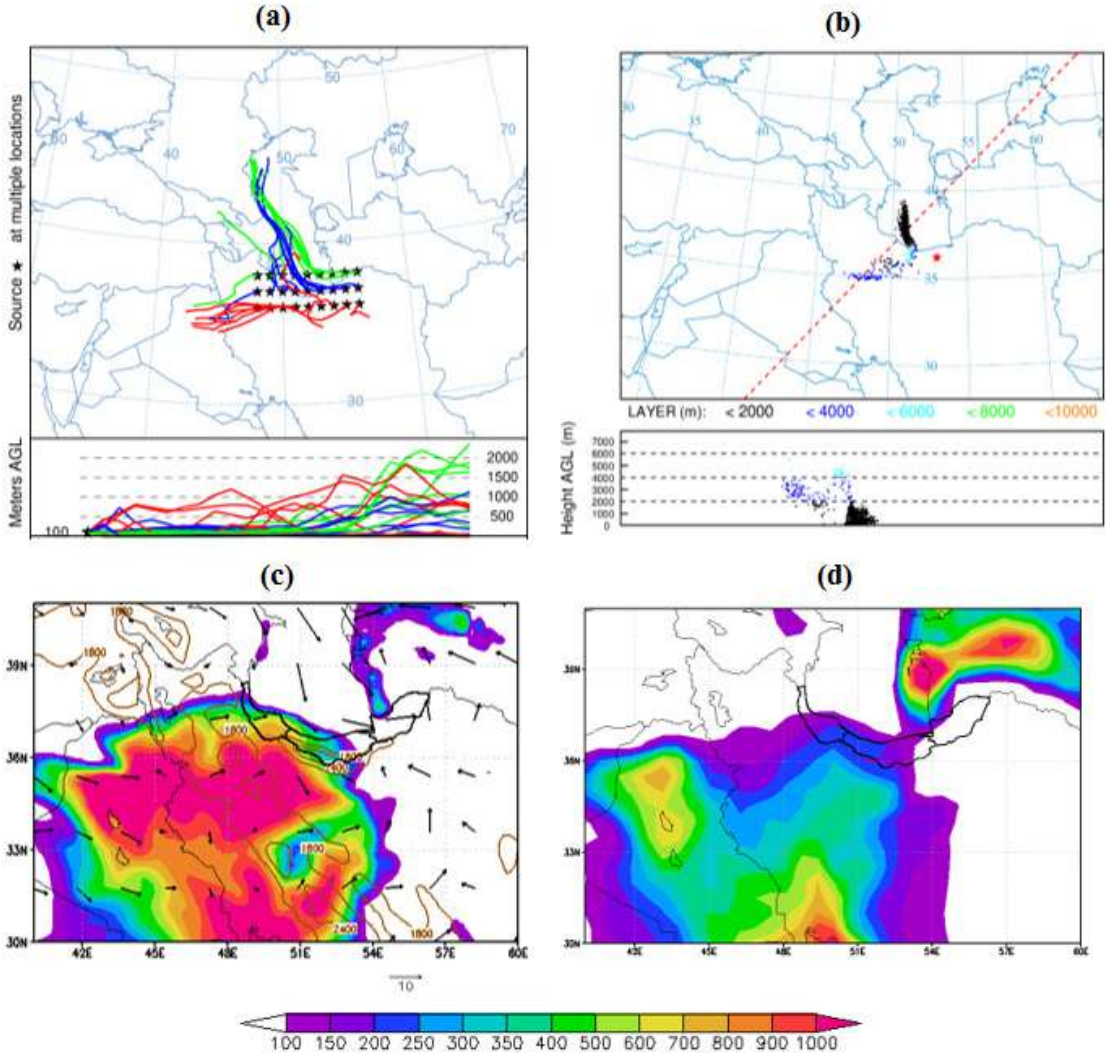

Fig. 14. The backward trajectory of HYSPLIT model at 100 m height for 18 h, at 12 UTC on May 24, 2022., b) The plume arrival (hours) from the initial time of the HYSPLIT dispersion model for the initial time of 12 UTC on May 24, 2022, c) The dust surface concentration and 10-m wind from the WRF-Chem model output, which was implemented from 12 UTC on April 6 as the initial time, d) the dust surface concentration from MERRA2 reanalysis data for 00 UTC on May 24, 2022.

In general, due to the forests and suitable vegetation on the southern shores of the Caspian Sea, the possibility of local dust storms is very small [32]; according to the results of this research, dust in the northern provinces are emitted from three sources in the north of Iraq, the central regions of Iran and Turkmenistan. This result is in agreement with many previous studies [15, 33].

The synoptic analysis resulted that in most case studies, there was a trough over the region, and the upward movements in front of its axis caused the transport of dust particles to higher levels of the atmosphere, resulting in higher wind speeds at these levels, over greater distances. [12] stated that in the transmission of dust to the southern shores of the Caspian Sea from Iraq and northern Saudi Arabia, upper

level waves and 500hPa currents play the most important role. The presence of a trough on the southern shores of the Caspian Sea causes the strengthening of low-pressure and the vertical expansion of dust to cross the Alborz mountain range and penetrate into the central Gilan plain and spread towards the Caspian Sea.

The dust reached by the currents of the atmosphere mid-levels is not able to pass through the high mountain chains in the study area, but due to the existence of some Valleys, the dust penetrates into the southern shores of the Caspian Sea and spreads towards the Sea [12].

Although the WRF-Chem model was able to predict dust transport to the southern coast of the Caspian Sea well in these case studies, it still has a large error in predicting dust concentrations in these areas. Since land surface data and meteorological quantities are effective in the accuracy of dust prediction output, it is difficult and complicated to identify the exact error factor [34, 35].

Conclusion

In this study, three cases of severe and wide spread dust in the southern shores of the Caspian Sea were investigated. In the true color images of the MODIS/Terra satellite, the dust mass with clouds can be seen in a large part of the southern Caspian Sea and its southern and eastern coasts. Some meteorological stations located in the north of Iran reported the dust phenomenon along with a decrease in visibility. Dust RGB images show dust in different hours in the eastern regions of Iraq, western, northwestern, northern and central Iran, as well as the eastern shores of the Caspian Sea located in western Turkmenistan. According to CALIPSO products, there was dust-type aerosols in a large part of the region near the ground to a height of about 6 km. At higher altitudes, especially over the Caspian Sea, it was cloudy, and dust particles were also shown at the bottom and between the clouds, although, due to cloud cover in a large part of area, there was not any dust data. However, AOD values were significant in the western Iraq, central areas of Iran, eastern shores of Caspian Sea located in western Turkmenistan, northern Caspian Sea and some points of southern shores of Caspian Sea.

Examining the synoptic patterns shows that the formation of surface low pressure over the Black Sea extending to Iraq and Saudi Arabia caused the Iran to be affected by troughs of these systems. The formation of high pressure over Russia and its extension to the Caspian Sea caused a strong pressure gradient and strong winds, so that the emission of dust from Iraq to the northwest of Iran and the southern shores of the Caspian Sea was observed. In addition, the low pressure in the central regions of Iran (south of Semnan and north of Isfahan) with strong winds caused the dust emission from the central regions of Iran and its transfer to the northeast of Iran. On the other hand, the dust source over Turkmenistan with the formation of another low pressure in this region emitted dust and transferred it towards the east of the Caspian Sea. At 500hPa level, height trough stretches from the Black Sea to the Red Sea. The southwesterly winds in the western regions of Iran directed the dust towards the northwestern regions of Iran and the southwestern coasts of the Caspian Sea. At the same time, the jet stream also caused instability in the lower levels of the atmosphere.

According to the output of the HYSPLIT model, a major part of the dust from the northern regions of Iraq entered the northwestern regions of Iran through the westerly and southwesterly currents and from there entered the southern shores of the Caspian Sea with the westerly currents. Of course, the presence of southerly and south-westerly winds in Mazandaran province caused the transfer of dust from the central regions of the country to this part as well. In addition, in

the eastern half of the southern shores of the Caspian Sea, the northerly and northwesterly currents transferred the dust from the west of Turkmenistan to these areas as well as the southern areas of the Caspian Sea.

Comparing the dust surface concentration output of the WRF-Chem model with the MERRA2 reanalysis data shows that this model was able to predict the dust transfer from Iraq to the west and northwest of Iran and then to the southern shores of the Caspian Sea. It performed well in predicting dust transfer from the central regions of Iran and western Turkmenistan to these coasts. However, the WRF-Chem model accuracy is still not sufficient for quantitative comparison.

According to the results of this research, dust in the northern provinces are emitted from three sources in the north of Iraq, the central regions of Iran and Turkmenistan.

Financial supports

This study does not have any financial support.

Competing interests

The authors declare that there are not any actual or potential competing interests.

Acknowledgements

The authors express their gratitude to IRIMO for providing synoptic station data. We sincerely thank the ECMWF teams for supplying meteorological maps and EUMETSAT for the Dust RGB images from the MSG satellite. Appreciation is extended to the GFS forecast team for the valuable data used in running the WRF-Chem model. We are also grateful for the AOD and MERRA2 data, accessed through Giovanni (https://giovanni.sci.gsfc.nasa.gov/giovanni/). The CALIPSO and HYSPLIT model teams are highly appreciated for their invaluable products.

Ethical considerations

Ethical issues (Including plagiarism, Informed Consent, misconduct, data fabrication and/or falsification, double publication and/or submission, redundancy, etc) have been completely considered by the authors.

References

1. Jebali A, Zare M, Ekhtesasi MR, Jafari R. Investigating of change extent of horizontal visibility in regions affected by dust events in Yazd Province. Desert Management. 2020 Aug 22;8(15):21-36.

2. Jasim SA, Mohammadi MJ, Patra I, Jalil AT, Taherian M, Abdullaeva UY, et al. The effect of microorganisms (bacteria and fungi) in dust storm on human health. Reviews on Environmental Health. 2024 Mar 25;39(1):65-75.

3. Middleton N, Al-Hemoud A. Sand and Dust Storms: Recent Developments in Impact Mitigation. Sustainability. 2024 Aug 19;16(16):7121.

4. Garaga R, Vaishnavi A, Dammala PK. Climate Change and Desert Dust Storms Induced Public Health Impacts on Rural Inhabitants of Western India. InSustainability and Health Informatics: A Systems Approach to Address the Climate Action Induced Global Challenge 2024 Sep 24 (pp. 273-281). Singapore: Springer Nature Singapore.

5. Rashki A, Middleton NJ, Goudie AS. Dust storms in Iran–Distribution, causes, frequencies and impacts. Aeolian Research. 2021 Jan 1;48:100655.

6. Song C, Guo Z, Liu Z, Hongyun Z, Liu R, Zhang H. Application of photovoltaics on different types of land in China: Opportunities, status and challenges. Renewable and Sustainable Energy Reviews. 2024 Mar 1;191:114146.

7. Wang K, Sun L, Wang J, Liu L. The electricity, industrial, and agricultural sectors under changing climate: Adaptation and mitigation in China. National Science Open. 2024 Jan 1;3(1):20230023.

8. Broomandi P, Dabir B, Bonakdarpour B, Rashidi Y. Identification of dust storm origin in South–West of Iran. Journal of Environmental Health Science and Engineering. 2017 Dec;15:1-4.

9. Ahmadi Foroushani M, Opp C, Groll M. Investigation of Aeolian dust deposition rates in different climate zones of Southwestern Iran. Atmosphere. 2021 Feb 7;12(2):229.

10. Norouzi S, Khademi H, Ayoubi S, Cano AF, Acosta JA. Seasonal and spatial variations in dust deposition rate and concentrations of dust-borne heavy metals, a case study from Isfahan, central Iran. Atmospheric Pollution Research. 2017 Jul 1;8(4):686-99.

11. Hojati S, Khademi H, Cano AF, Landi A. Characteristics of dust deposited along a transect between central Iran and the Zagros Mountains. Catena. 2012 Jan 1;88(1):27-36.

12. Asadi Oskouei E, Negah S and Farid Mojtahedi N. Penetration and distribution of dust in west-southern coast of Caspian Sea. The 2nd International Conference on Plant, Water, Soil and Weather Modeling. 2013 Kerman, Iran.

13. Mostofie N, Fataei E, Hezhabrpour Gh KZ. Assessment centers and distribution centers dust(case study: NorthWest, Iran). International Journal of Farming and Allied Sciences. 2014;3(2):235-43.

14. Baghi M, Rashki A, Mahmudy Gharaie MH. Investigation of Chemical and Mineralogical Properties of Dust Entering Northeastern Iran and its Pathogenic Potential. Journal of Geography and Environmental Hazards. 2020 May 21;9(1):139-53.

15. Ghaffarian P, Negah S, Farid Mojtahedi N and Abed H. Simulation of fine dust emitted from the desert of Turkmenistan to the southern shores of the Caspian Sea. Applied Researches in Geographical Sciences. 2015;15(38):141-164.

16. Karami S, Ghassabi Z, Rezazadeh P. Investigating the mechanism of dust transferring from Iraq to the north of Alborz mountains in Iran. Journal of Air Pollution and Health. 2022 Dec 18;7(4):375-98.

17. Abdi Vishkaee F, Flamant C, Cuesta J, Oolman L, Flamant P, Khalesifard HR. Dust transport over Iraq and northwest Iran associated with winter Shamal: A case study. Journal of Geophysical Research: Atmospheres. 2012 Feb 16;117(D3).

18. Boloorani AD, Nabavi SO, Bahrami HA, Mirzapour F, Kavosi M, Abasi E, Azizi R. Investigation of dust storms entering Western Iran using remotely sensed data and synoptic analysis. Journal of Environmental Health Science and Engineering. 2014 Dec;12:1-2.

19. Momenpour F. Dust hazard in southwest area of Caspian Sea. Second International Conference on Environmental Hazards. 2012 Tehran, Iran.

20. Hong SY, Dudhia J, Chen SH. A revised approach to ice microphysical processes for the bulk parameterization of clouds and precipitation. Monthly weather review. 2004 Jan 1;132(1):103-20.

21. Mlawer EJ, Taubman SJ, Brown PD, Iacono MJ, Clough SA. Radiative transfer for inhomogeneous atmospheres: RRTM, a validated correlated-k model for the longwave. Journal of Geophysical Research: Atmospheres. 1997 Jul 27;102(D14):16663-82.

22. Chou MD, Suarez MJ. A solar radiation parameterization for atmospheric studies. 1999 Jun 1.

23. Chen F, Kusaka H, Tewari M, Bao JW, Hirakuchi H. Utilizing the coupled WRF/LSM/Urban modeling system with detailed urban classification to simulate the urban heat island

phenomena over the Greater Houston area. InFifth Symposium on the Urban Environment. 2004 Aug 23 (Vol. 25, pp. 9-11). American Meteorological Society Vancouver, BC, Canada.

24. Noh Y, Cheon WG, Hong SY, Raasch S. Improvement of the K-profile model for the planetary boundary layer based on large eddy simulation data. Boundary-layer meteorology. 2003 May;107:401-27.

25. Hong SY, Lim JO. The WRF single-moment 6-class microphysics scheme (WSM6). Asia-Pacific Journal of Atmospheric Sciences. 2006 Apr;42(2):129-51.

26. Grell GA. Prognostic evaluation of assumptions used by cumulus parameterizations. Monthly weather review. 1993 Mar;121(3):764-87.

27. Lin SJ. A "vertically Lagrangian" finite-volume dynamical core for global models. Monthly Weather Review. 2004 Oct 1;132(10):2293-307.

28. Bacmeister JT, Suarez MJ, Robertson FR. Rain reevaporation, boundary layer–convection interactions, and Pacific rainfall patterns in an AGCM. Journal of the Atmospheric Sciences. 2006 Dec 1;63(12):3383-403.

29. Koster RD, Suarez MJ, Ducharne A, Stieglitz M, Kumar P. A catchment-based approach to modeling land surface processes in a general circulation model: 1. Model structure. Journal of Geophysical Research: Atmospheres. 2000 Oct 27;105(D20):24809-22.

30. Stendel M, Francis J, White R, Williams PD, Woollings T. The jet stream and climate change. InClimate change 2021 Jan 1 (pp. 327-357). Elsevier.

31. Hamzeh NH, Karami S, Kaskaoutis DG, Tegen I, Moradi M, Opp C. Atmospheric dynamics and numerical simulations of six frontal dust storms in the Middle East region. Atmosphere. 2021 Jan 18;12(1):125.

32. Sobhani B, Jafarzadeh Aliabad L, Mohamadi GH. Investigating the horizontal visibility characteristics in the southern coasts of the Caspian Sea using the extinction coefficient. Journal of Environmental Science Studies. 2024 Oct 22;9(2):8466-51.

33. Rashki A, Kaskaoutis DG, Sepehr A. Statistical evaluation of the dust events at selected stations in Southwest Asia: From the Caspian Sea to the Arabian Sea. Catena. 2018 Jun 1;165:590-603.

34. Karami S, Kaskaoutis DG, Kashani SS, Rahnama M, Rashki A. Evaluation of nine operational models in forecasting different types of synoptic dust events in the Middle East. Geosciences. 2021 Nov 7;11(11):458.

35. Kishcha P, Alpert P, Shtivelman A, Krichak SO, Joseph JH, Kallos G, Katsafados P, Spyrou C, Gobbi GP, Barnaba F, Nickovic S. Forecast errors in dust vertical distributions over Rome (Italy): Multiple particle size representation and cloud contributions. Journal of Geophysical Research: Atmospheres. 2007 Aug 16;112(D15).